Applied Catalysis B: Environmental 144 (2014) 855–862

Contents lists available at ScienceDirect

Applied Catalysis B: Environmental

journal homepage: www.elsevier.com/locate/apcatb

Pt-loading reverses the photocatalytic activity order of anatase TiO_2 {0 0 1} and {0 1 0} facets for photoreduction of CO_2 to CH_4

Jin Mao [1], Liqun Ye [1], Kan Li, Xiaohu Zhang, Jinyan Liu, Tianyou Peng *, Ling Zan *

College of Chemistry and Molecular Science, Wuhan University, Wuhan 430072, PR China

ARTICLE INFO

Article history:
Received 22 March 2013
Received in revised form 12 August 2013
Accepted 15 August 2013
Available online 28 August 2013

Keywords:
Photoreduction of CO_2
TiO_2 {0 0 1} and {0 1 0} facets
Pt-loading
Photocatalytic activity

ABSTRACT

It is well known that different crystal facets of TiO_2 have different surface electronic and atomic structures, which can influence the photocatalytic performance, and appropriate noble metal-loading usually improves the photocatalytic activity. Herein we demonstrate that Pt-loading can reverse the photocatalytic activity order of anatase TiO_2 {0 0 1} facets (TiO_2-0 0 1) and {0 1 0} facets (TiO_2-0 1 0) for the photoreduction of CO_2 to CH_4. This new phenomenon was discussed on the bases of the experimental data including attenuated total reflectance Fourier transform infrared (ATR-IR) spectra, CO_2 temperature programmed desorption (CO_2-TPD) curves, transmission electron microscopy (TEM) images and time-resolved photoluminescence (PL) spectra. It is found that the higher photocatalytic CO_2 reduction activity of TiO_2-0 1 0 without Pt-loading can be attributed to its larger CO_2 adsorbed amount and longer charge lifetime as compared with TiO_2-0 0 1, while the Pt nanoparticles loaded on TiO_2-0 0 1 can more efficiently enhance the photoinduced carrier separation efficiency than that on TiO_2-0 1 0, and therefore resulting in a photoactivity higher than the Pt-loaded TiO_2-0 0 1. The above results provide an important indication about the effects of Pt-loading on the photocatalytic CO_2 reduction activity of anatase TiO_2 with different exposed facets, and shed light on the fabrication of novel nanostructured photocatalysts through morphological control for high conversion efficiency in the CO_2 resource utilization.

1. Introduction

Global climate change caused by increasing atmospheric CO_2 concentration due to the consumption of fossil fuels is the main problem for the sustainable development of human beings. Converting CO_2 to useful hydrocarbon fuels with solar energy is an attracting strategy, which can provide a package solution to the above problems by utilizing inexhaustible solar energy. Although many photocatalysts have been developed and applied to the photocatalytic CO_2 reduction in an aqueous suspension to produce organic fuels such as methanol (CH_3OH), formic acid (HCOOH) and methane (CH_4) [1–7], those hydrosoluble products (for example CH_3OH) derived from the aqueous suspension usually serves as hole scavenger during a long-term reaction, which affects the accumulation of those hydrocarbon product and the overall conversion efficiency. In recent years, some examples with more practical significance are focused on gaseous phase reaction in a heterogeneous photocatalytic CO_2 reduction system containing photocatalyst and H_2O vapor [8–12]. Generally, the photocatalytic CO_2 reduction efficiencies of those gaseous phase reactions are mainly depended on two factors: the CO_2 adsorption capability on the photocatalyst surfaces and the photoinduced electron transfer efficiency toward CO_2. The surface characteristics of photocatalyst are thus very important factors influencing the photocatalytic CO_2 reduction activity in the gaseous phase CO_2 photoreduction system.

On the other hand, it is well known that different crystal facets of TiO_2 possess different surface electronic and atomic structures, which usually dominate the redox potentials of the photogenerated carriers and the surface active sites of the adsorbed reactant molecules, and then resulting in different photoactivities [13–16]. For example, Cheng's group have reported that single crystal anatase TiO_2 nanorods with dominant reactive {0 1 0} facets showed a higher photoactivity for converting CO_2 into CH_4 than the benchmark P25 (TiO_2 nanoparticles) with 1 wt% Pt-loading under Xe-lamp irradiation [14]. Usually, the size and shape of Pt nanoparticles loaded on TiO_2 closely depend on the surface electronic structure of TiO_2 [15,16]. In other words, the different facets may influence the morphology, size and distribution of the Pt nanoparticles loaded on TiO_2 surfaces, and therefore it can be conjectured that the Pt-loading would play an important role during the CO_2 photoreduction over TiO_2 with different exposed facets. However, there are only a few researches about the effects of Pt-loading on the photoactivity of anatase TiO_2 with different exposed facets for the CO_2 photoreduction to the best of our knowledge.

* Corresponding authors.
E-mail addresses: typeng@whu.edu.cn (T. Peng), irlab@whu.edu.cn (L. Zan).
[1] The authors contributed equally.

0926-3373/$ – see front matter © 2013 Elsevier B.V. All rights reserved.
http://dx.doi.org/10.1016/j.apcatb.2013.08.027

Herein, anatase TiO_2 samples with exposed {0 0 1} facets and {0 1 0} facets were synthesized, which were denoted as TiO_2-0 0 1 and TiO_2-0 1 0, respectively. It is found that 1 wt% Pt-loading can reverse the photocatalytic activity order of anatase TiO_2 {0 0 1} and {0 1 0} facets for the photocatalytic CO_2 conversion to CH_4. Namely, TiO_2-0 1 0 without Pt-loading shows a higher photocatalytic CO_2 reduction activity than TiO_2-0 0 1; while TiO_2-0 1 0 with 1 wt% Pt-loading displayed a lower photoactivity than TiO_2-0 0 1 with 1 wt% Pt-loading. This novel phenomenon was explored and elucidated by the experimental data with the aid of various characterization techniques and the corresponding mechanism reported previously.

2. Experimental

2.1. Preparation

TiO_2-0 0 1: Anatase TiO_2 with exposed {0 0 1} facets (TiO_2-0 0 1) was hydrothermally prepared *via* a procedure similar to the previous report [17]. Typically, tetrabutoxytitanium (IV) ($Ti(OBu)_4$, 10 mL) and hydrofluoric acid aqueous solution (37%, 3 mL) were mixed in a dried Teflon-lined autoclave (50 mL) under ambient conditions, and then the autoclave was tightened and kept at 200 °C for 24 h. The white product was filtrated and subsequently washed with deionized water and ethanol three times, and then dried at 60 °C for 10 h to obtain anatase TiO_2 with exposed {0 0 1} facets (TiO_2-0 0 1). Finally, the TiO_2-0 0 1 was calcined at 600 °C for 2 h to remove the surface fluorine.

TiO_2-0 1 0: Anatase TiO_2 with exposed {0 1 0} facets (TiO_2-0 1 0) was synthesized by using a reported route [14,18,19]. Firstly, 1.0 g of P25 (TiO_2 nanoparticles, Degussa) was added into 10 M NaOH solution (40 mL) under stirring, the resulting suspension was transferred into Teflon-lined autoclave (50 mL), and then the autoclave was tightened and kept at 200 °C for 24 h. The white precipitate was collected by centrifugation to obtain sodium titanate (ST). Secondly, 1.0 g of the above sodium titanate (ST), which is isolated by centrifugation without drying, was dispersed into 2% H_2O_2 solution (35 mL), and then transferred into a Teflon-lined autoclave (50 mL). The autoclave was tightened and kept at 180 °C for 24 h. The white production was filtrated and subsequently washed with deionized water three times, and then dried at 60 °C for 10 h to obtain anatase TiO_2 with exposed {0 1 0} facets (TiO_2-0 1 0).

Pt-loading: The platinization of anatase TiO_2 is carried out according to a typical photodeposition method. 0.2 g of the as-prepared TiO_2 samples was dispersed into 40 mL distilled water under vigorous stirring, and then 10 mL methanol and 0.13 mL H_2PtCl_6 (0.077 M) solution were added to the suspension in sequence. The mixture was irradiated by a 500 W high-pressure Hg-lamp for 3 h under continuous stirring. After centrifugation, the sample was washed with water and dried at 80 °C for 10 h to obtain 1 wt% Pt-loaded TiO_2. The obtained 1 wt% Pt-loaded anatase TiO_2-0 0 1 and TiO_2-0 1 0 were denoted as TiO_2-0 0 1-1%Pt and TiO_2-0 1 0-1%Pt, respectively. For comparison, 5 wt% Pt-loaded TiO_2-0 0 1 and TiO_2-0 1 0 were also prepared by using the same method, and denoted as TiO_2-0 0 1-5%Pt and TiO_2-0 1 0-5%Pt, respectively.

2.2. Material characterization

X-ray diffraction patterns (XRD) of the samples were recorded on a Bruker D8 advance X-ray diffractometer by using Cu Kα radiation ($\lambda = 0.1542$ nm) and 2θ scan rate of 6° min^{-1} in the range of $20° \leq 2\theta \leq 70°$. X-ray photoelectron spectroscopy (XPS) measurements were carried out by using VG Multilab 2000 spectrometer (Thermo Electron Corp.) with an Mg Kα X-ray source, and the XPS spectra were calibrated to the C 1s peak at 284.6 eV Morphology and microstructures of samples were observed by using a JEOL JEM-6700F Field Emission Scanning Electron Microscope (FESEM) operated at an accelerating voltage of 15 kV and applied current of 10 mA, and a JEOL JEM-2000 (RH) high-resolution transmission electron microscope (HRTEM) operated at an accelerating voltage of 200 kV. The time-resolved photoluminescence (PL) spectra were recorded by a Multifunction Steady State and Transient State Fluorescence Spectrometer (FES920, Edinburgh Instruments) at 398 nm with 330 nm excitation. N_2 adsorption–desorption measurement was performed on a Micrometrics ASAP2020 at 77 K after the sample was degassed at 120 °C.

Attenuated total reflectance infrared (ATR-IR) spectra in the presence of H_2O vapor were recorded on a Bruker VERTEX 70 spectrometer equipped with a liquid cooled MCT detector. According to the photoactivity test process, 0.1 g of photocatalyst was uniformly dispersed onto the watch-glass in a reaction cell, which was then thoroughly vacuum-treated to remove air completely, and then supercritical fluid-grade CO_2 gas was introduced into the reactor until 1 atm. After then 1 mL of deionized water was injected into the reaction cell, which was not in contact with the photocatalyst, and then kept for 60 min to adsorb CO_2 and H_2O vapor in the dark. The background was collected by using an untreated sample at room temperature (20 °C). Approximately 4 mg of the above sample was pressed onto a cell for the ATR-IR test, which was used together with an ATR accessory for infrared spectrum measurement with an IR scanning range of 4000–800 cm^{-1} and 4 cm^{-1} resolution by using 32 scans. Moreover, the above photocatalyst (47.5 mg) after the adsorption process was also applied to test of the CO_2 temperature programmed desorption (CO_2-TPD) curves by using Micromeritics Autochem 2. The sample was firstly heated to 50 °C in flowing Ar for 30 min, and then the sample was heated to 800 °C at a heating rate of 10 °C min^{-1} under Ar flowing.

2.3. Photocatalytic reduction of CO_2

The photocatalytic CO_2 reduction was carried out in a home-made closed gas system. In the photocatalytic CO_2 reduction reaction system, 0.1 g of photocatalyst was uniformly dispersed onto the watch-glass with an area of ~28 cm^2, which was then put in the reaction cell (Pyrex glass) with a total volume of 350 mL. Prior to the light irradiation, the above system was thoroughly vacuum-treated to completely remove air. After that, supercritical fluid-grade CO_2 gas (Minghui technical gases, Wuhan, China) was introduced into the reactor until 1 atm, and then 1 mL of deionized water was injected into the reactor as the reductant, which was then kept for 30 min to establish an adsorption–desorption balance. After that, the reactor was irradiated from the top by 300 W Hg-lamp (Changzhou Yuyu Electro-Optical Device Co., Ltd. China), and the photoreaction temperature was kept at 20 °C. During the irradiation, about 0.25 mL of gas was taken from the reaction cell for subsequent qualitative analysis by using SP 6800A gas chromatography (GC) equipped with flame ionization detector (GC-FID, GDX-502 columns) and thermal conductivity detector (GC-TCD, TDX-01 columns). The quantification of the production yield was based on a calibration curve. The outlet gases were determined to be CH_4, O_2 and CO_2 but no CO, H_2 or other hydrocarbons.

3. Results and discussion

3.1. Microstructure and crystal phase analyses of photocatalyst

Fig. 1 shows the X-ray diffraction patterns (XRD) patterns of the obtained TiO_2 samples with or without 1 wt% Pt-loading. As can be seen, the reflection peaks located at $2\theta = 25.4°$, 37.8°, 48.5°, 54.0°, 55.4° and 62.9° for those four samples can be indexed to (1 0 1), (0 0 4), (2 0 0), (1 0 5), (2 1 1) and (2 0 4) crystal facets of

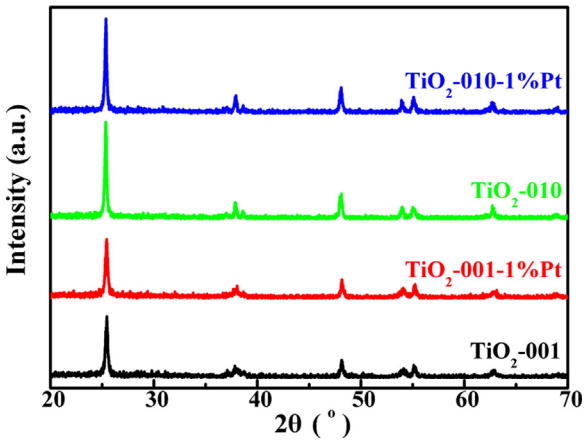

Fig. 1. XRD patterns of TiO_2-0 0 1, TiO_2-0 0 1-1%Pt, TiO_2-0 1 0 and TiO_2-0 1 0-1%Pt.

tetragonal anatase TiO_2 (JCPDS No. 21-1272), respectively. Moreover, no diffraction peak for any other crystal phase of TiO_2 can be observed in those XRD patterns, demonstrating the formation of pure anatase TiO_2. Nevertheless, there is no reflection peak attributable to the Pt for the TiO_2-0 0 1-1%Pt and TiO_2-0 1 0-1%Pt, which may be due to the low content and high dispersity of the loaded Pt particles.

FESEM image shown in Fig. 2a reveals that the obtained TiO_2-0 1 0 is mainly composed of nanorods with particle size of *ca.* 1000 × 100 nm and *ca.* 93% exposed percentage of {0 1 0} facets, and its HRTEM image (the inset in Fig. 2b) shows the [0 1 0] orientation of the nanorod and the clear lattice fringes with lattice spacing of 0.48 and 0.35 nm, corresponding to the {0 0 2} and {1 0 1} facets of anatase TiO_2, respectively. The angles of {1 0 1}–{1 0 −1} facets and {1 0 1}–{0 0 2} facets can be estimated to be *ca.* 44° and 68°, which are in agreement with the corresponding fast Fourier transform (FFT) pattern (the inset in Fig. 2b). Therefore, it can be concluded that the four rectangle facets of the nanorod are {0 1 0} facets of anatase TiO_2 since {0 1 0} and {1 0 0} facets have the same surface construction. Similarly, FESEM image shown in Fig. 2c indicates that TiO_2-0 0 1 is composed of nanosheets with size of *ca.* 200 × 10 nm and *ca.* 91% exposed percentage of {0 1 0} facets, and its HRTEM image (the inset in Fig. 2d) displays the [0 0 1] orientation and two clear lattice fringes with a lattice spacing of 0.20 nm, corresponding to the {0 2 0} and {2 0 0} facets, and the angle between them is 90°, which agrees well with the FFT pattern (the inset in Fig. 2d). Therefore, the two square facets (top and bottom facets) of the TiO_2 nanosheets are {0 0 1} facets.

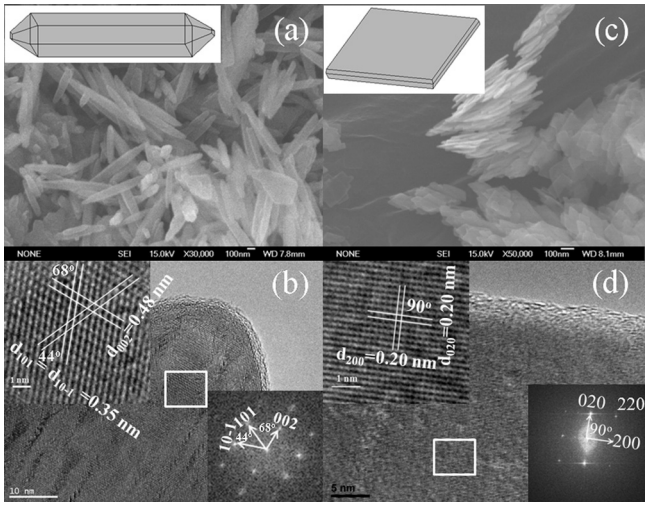

Fig. 2. FESEM and HRTEM images of TiO_2-0 1 0 (a and b) and TiO_2-0 0 1 (c and d). The insets in (b) and (d) are the corresponding FFT patterns of TiO_2-0 1 0 and TiO_2-0 0 1, respectively.

The X-ray photoelectron spectra (XPS) were obtained to analyze the oxidization state and the surface chemical composition of TiO_2-0 0 1-1%Pt and TiO_2-0 1 0-1%Pt. As can be seen from the survey XPS spectra in Fig. 3a, there are Ti, O, C and Pt elements existing in both the samples. The binding energy (BE) values were corrected by assigning the value of 284.6 eV to the C 1s peak of adventitious hydrocarbons; it can be found that there is a very weak peak of C 1s located at 284.6 eV The binding energy values of Pt 4f7/2 and 4f5/2 can be observed to be 72.1 and 75.3 eV as shown in Fig. 3b, which are almost equal to the standard binding energy of metallic Pt, indicating that Pt metal particles loaded on TiO_2 surfaces for TiO_2-0 0 1-1%Pt and TiO_2-0 1 0-1%Pt by using the present photodeposition method. Moreover, the TiO_2-0 0 1 is shown to be fluoride-free crystals as can be observed from the XPS spectra in Fig. 3c [17,20,21], and the Brunauer–Emmett–Teller (BET) specific surface areas of TiO_2-0 0 1 and TiO_2-0 1 0 are measured to be 67.4 and 32.9 $m^2\ g^{-1}$, respectively.

3.2. Photocatalytic CO_2 reduction activity analyses

Control experiments showed no appreciable reduced C1 or C2 products detected in the absence of either photocatalyst or light irradiation, illustrating that both photocatalyst and light irradiation are necessary for the present gaseous photocatalytic CO_2 reduction process, and the primary experimental results showed CH_4 was the main product from the gaseous photocatalytic CO_2 reduction systems by using TiO_2-0 0 1, TiO_2-0 1 0, TiO_2-0 0 1-1%Pt or TiO_2-0 1 0-1%Pt as photocatalyst in the presence of H_2O vapor. Moreover, when the photocatalytic system was illuminated by introducing N_2 instead of CO_2 into the reactor, neither CH_4/CO nor other carbon-containing organic compounds can be observed. The above results demonstrated that the generation of CH_4 product was stemmed from the photocatalytic CO_2 reduction process, and the selective formation of CH_4 rather than other hydrocarbons (such as CH_3OH and CO) might be ascribed to its more feasible thermodynamics because the redox potential of CO_2/CH_4 [$E^\circ(CO_2/CH_4) = -0.24$ V *vs.* NHE, pH7.00] is much lower than that of CO_2/CO [$E^\circ(CO_2/CO) = -0.53$ V *vs.* NHE, pH7.00] or CO_2/CH_3OH [$E^\circ(CO_2/CH_3OH) = -0.38$ V *vs.* NHE, pH 7.00] [15,21].

Fig. 4 depicts the CH_4 production amount from the above photocatalytic system containing different photocatalysts under UV-light irradiation for 2 h. As can be seen, TiO_2-0 0 1 shows a lower photocatalytic CO_2 reduction activity for CH_4 production than TiO_2-0 1 0, and 1 wt% Pt-loading leads to a significant increment in the CH_4 production for TiO_2-0 0 1. However, the 1 wt% Pt-loading obviously retards the photocatalytic CO_2 reduction activity of TiO_2-0 1 0, rendering its photoactivity inferior to the Pt-loaded TiO_2-0 0 1. Namely, Pt-loading can reverse the photoactivity order of anatase TiO_2 {0 0 1} and {0 1 0} facets during the photoreduction of CO_2 to CH_4.

To further confirm this phenomenon on Pt-loading, the CH_4 evolution efficiency over 5 wt% Pt-loaded samples (TiO_2-0 0 1-5%Pt and TiO_2-0 1 0-5%Pt) under UV-light irradiation for 4 h were estimated and shown in Fig. 5, and a similar reversing trend in the photoactivity order of anatase TiO_2 {0 0 1} and {0 1 0} facets can also be observed. Therefore, it might be conjectured that the above effect of Pt-loading on the photoactivity is largely attributed to the difference of crystal facets rather than the Pt-loaded level.

3.3. Reason analyses of the reversed photocatalytic activity order by Pt-loading

In order to reveal the origin of the reversed photoactivity order of TiO_2-0 0 1 and TiO_2-0 1 0 after the Pt-loading, ATR-IR, CO_2-TPD

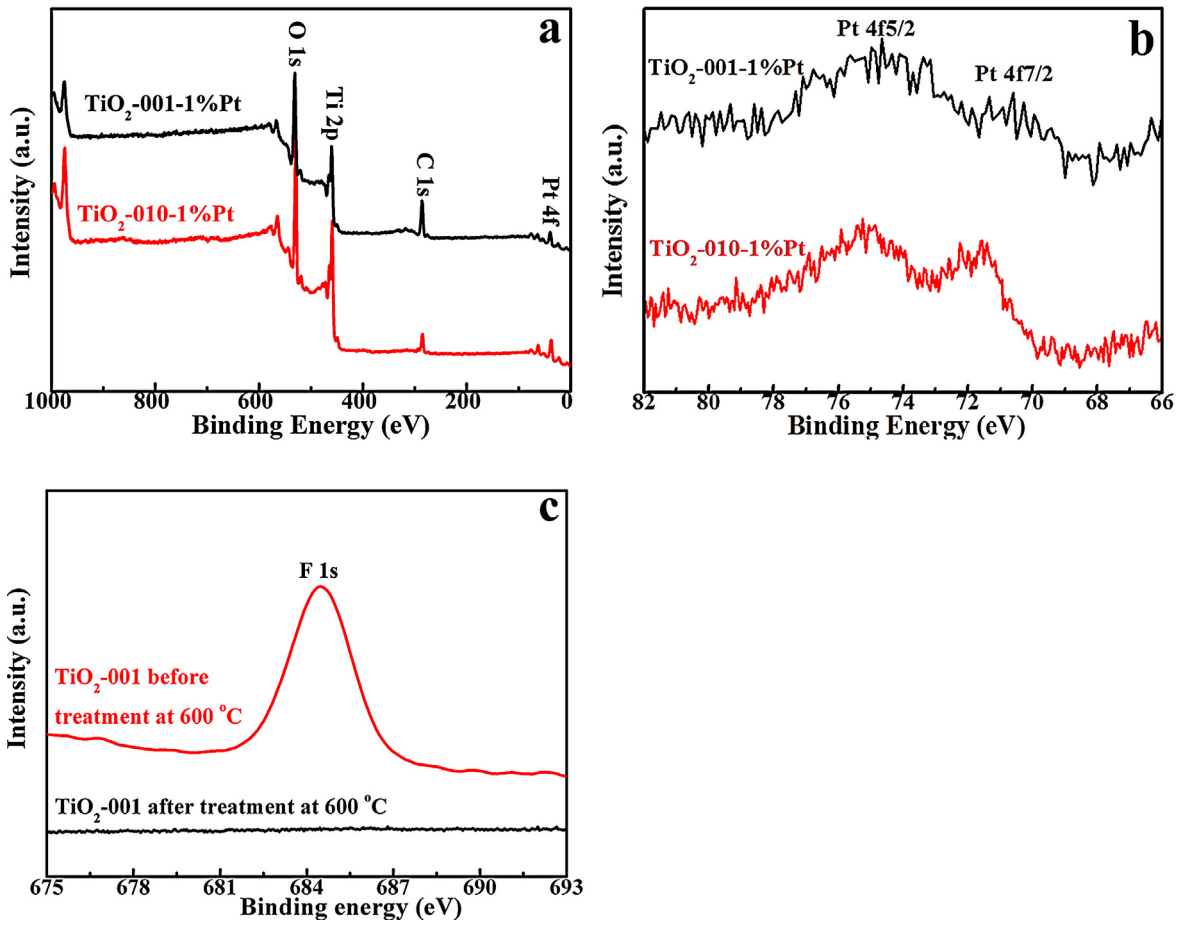

Fig. 3. Survey (a) and Pt4f (b) XPS spectra of TiO_2-0 0 1-1%Pt and TiO_2-0 1 0-1%Pt, and TiO_2-0 0 1 before and after the heat treatment at 600 °C (c).

and time-resolved PL spectra were used to investigate the CO_2 adsorption and the corresponding charge transfer properties during the present photocatalytic process. ATR-IR spectra (Fig. 6a) of TiO_2-0 1 0 and TiO_2-0 0 1 were recorded after CO_2 adsorption for 1 h in the presence of H_2O vapour. It can be found that monodentate carbonate ($m\text{-}CO_3^{2-}$) and bicarbonate (HCO_3^-) are formed on both TiO_2-0 1 0 and TiO_2-0 0 1 [22–25], and TiO_2-0 1 0 shows more active and effective CO_2 adsorption than TiO_2-0 0 1 in the presence of H_2O vapour in terms of the corresponding IR peak intensities shown in Fig. 6a. This result was also confirmed by the CO_2-TPD curves shown in Fig. 6b, which is usually applied to survey the adsorption amount and the base strength of catalysts. The desorption peaks in the temperature region between 250 and 450 °C may be attributed to the CO_2 desorption from weak bases sites such as bicarbonates, while the main peak in the range of 500–600 °C may be due to the decomposition of the strongly adsorbed carbonates [26–30]. By comparing the peak areas of those CO_2 desorption and the variance of peak maximum temperature, it can be concluded that the CO_2 adsorbed amount on TiO_2-0 1 0 is larger than that on TiO_2-0 0 1. This leads to the judgement that TiO_2-0 1 0 surfaces is more favorable to the coverage and adsorption of CO_2-derived species, which then would result in its better photoactivity for the CO_2 photoreduction as compared to TiO_2-0 0 1. Furthermore, the charge lifetime (0.71 ns) of TiO_2-0 1 0 is slightly longer than that (0.65 ns) of TiO_2-0 0 1 according to the time-resolved PL spectra shown in Fig. 6c, indicating that TiO_2-0 1 0 has more efficient photogenerated carrier separation efficiency than TiO_2-0 0 1.

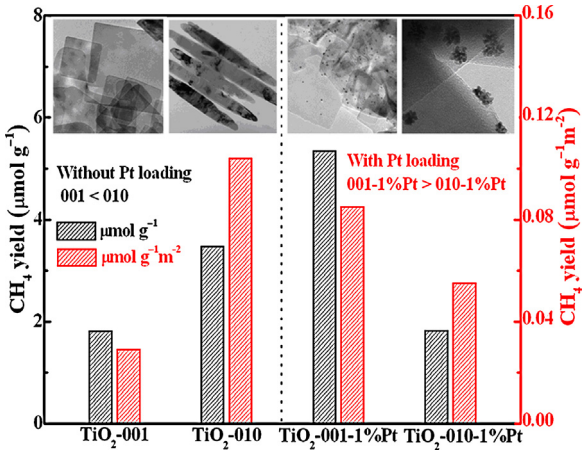

Fig. 4. Photocatalytic reduction activity of CO_2 to CH_4 over TiO_2-0 0 1, TiO_2-0 1 0, TiO_2-0 0 1-1%Pt and TiO_2-0 1 0-1%Pt under UV-light irradiation for 2 h.

Usually, the criteria used to predict the photoactivity of crystal facets is the surface unsaturated coordinated atom density [17,20]. Among the three fundamental low-index facets ({0 0 1}, {0 1 0} and {1 0 1}) of the anatase TiO_2 crystals, both {0 0 1} and {0 1 0} facets containing 100% unsaturated five-coordinated Ti (Ti5c) atoms at their surfaces are theoretically considered more reactive than {1 0 1} facets containing 50% Ti5c atoms and 50% saturated coordinated Ti (Ti6c) atoms in terms of the surface Ti5c atom percentage [20]. On the contrary, {0 1 0} and {1 0 1} facets should have photoreactivity superior to {0 0 1} facets when considering that more strongly reductive electrons can be generated on {0 1 0} and {1 0 1} facets because their CB minimum in the order {1 0 1} ≈ {0 1 0} > {0 0 1} [20]. Obviously, {0 1 0} facets have both a

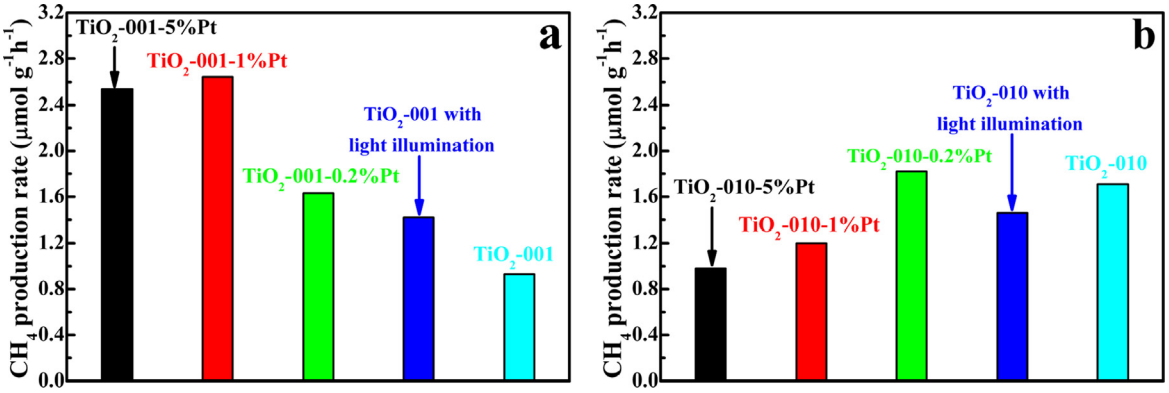

Fig. 5. Photocatalytic reduction activity of CO_2 to CH_4 over TiO_2-0 0 1 and TiO_2-0 1 0 and their corresponding 1 wt% or 5 wt% Pt-loaded products under UV-light irradiation for 4 h.

favorable surface atomic structure and a surface electronic structure, so that the more strongly reducing electrons in the CB of the {0 1 0} facets can be transferred *via* the surface Ti5c atoms as active reaction sites [20]. The efficient consumption of excited electrons in the photoreduction reactions can simultaneously promote the holes involved in photooxidation reactions [20], and then resulting in the above longer charge lifetime of TiO_2-0 1 0 as compared to the TiO_2-0 0 1. Such a collaborative mechanism existing on {0 1 0} facets is responsible for the higher reactivity than the {0 0 1} facets. It therefore can be concluded that the better photocatalytic CO_2 reduction activity of TiO_2-0 1 0 might stem from its higher CO_2 adsorption capability and more efficient charge transfer capability than TiO_2-0 0 1.

Nevertheless, all these observations on ATR-IR, CO_2-TPD and time-resolved PL spectra were reversed after 1 wt% Pt-loading on those facets. As can be seen from Fig. 7a, TiO_2-0 0 1-1%Pt was still dominated by m-CO_3^{2-} and HCO_3^-, while bidentate carbonate (b-CO_3^{2-}) with very strong peak in addition to the m-CO_3^{2-} and HCO_3^- were mainly formed on the TiO_2-0 1 0-1%Pt, which is significantly different from the unloaded TiO_2-0 1 0 as shown in Fig. 6a. According to the previous reports [31–34], the above changes may be due to the surface reconstruction of different facets under the

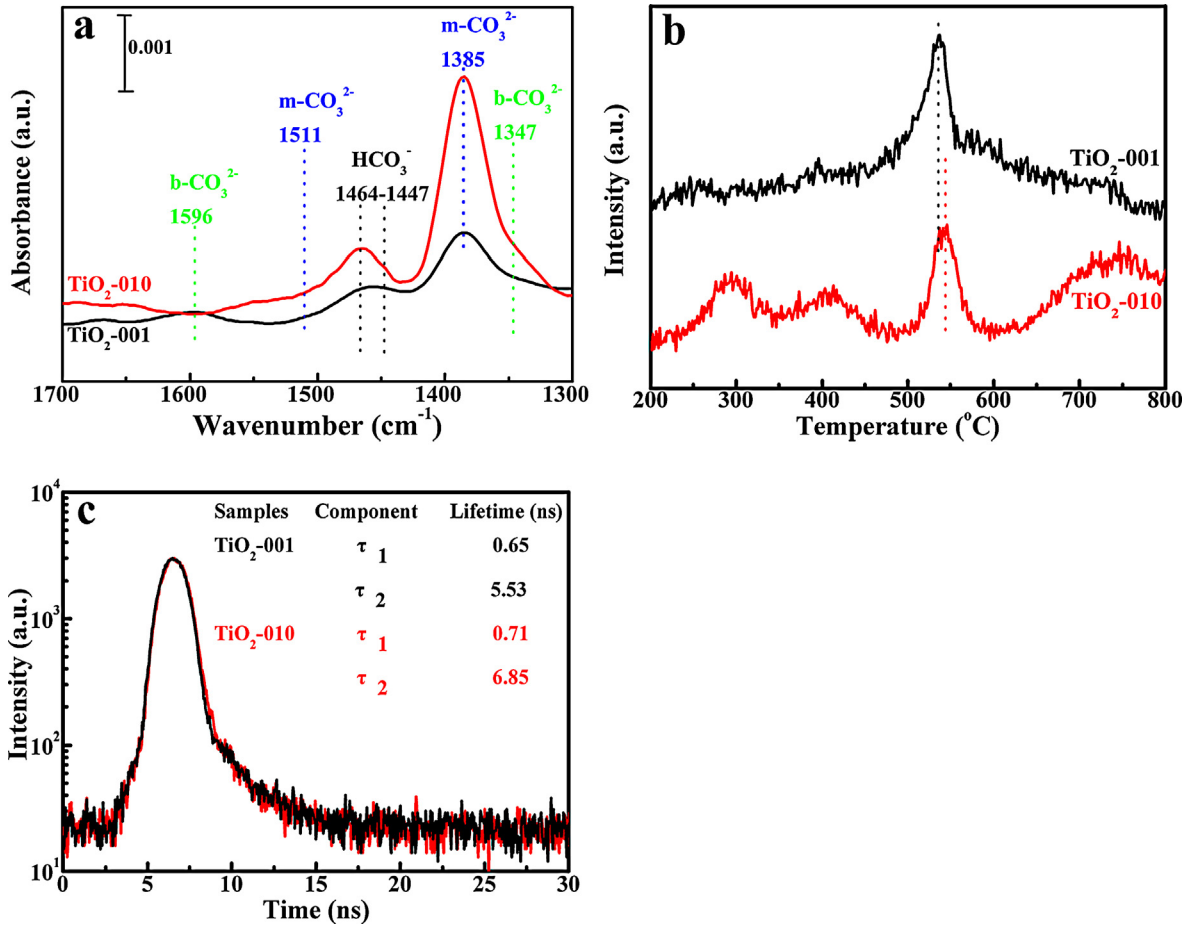

Fig. 6. ATR-IR spectra (a), CO_2-TPD curves (b), and time-resolved PL spectra (c) of TiO_2-0 0 1 and TiO_2-0 1 0.

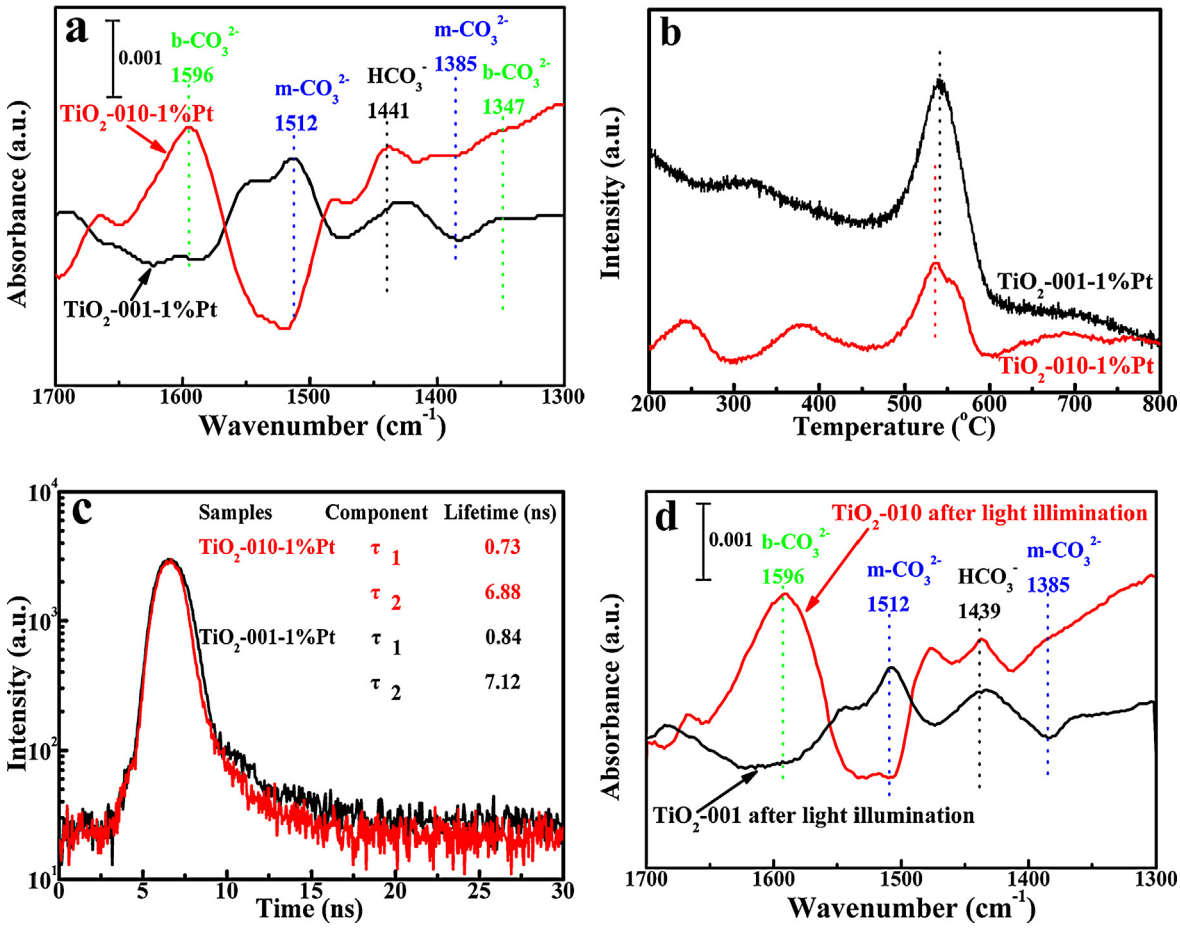

Fig. 7. ATR-IR spectra (a), CO_2-TPD curves (b), and time-resolved PL spectra (c) of TiO_2-0 0 1-1%Pt and TiO_2-0 1 0-1%Pt, and the ATR-IR spectra (d) of TiO_2-0 0 1 and TiO_2-0 1 0 after the intensive UV-light illumination without Pt-loading.

present intense UV-light irradiation during the Pt deposition process because it has been reported that the possible influence of surface reconstruction on the photoactivity of different facets [20]. Of course, the different TiO_2 facets may also influence the morphology, size and distribution of the Pt nanoparticles loaded on their surfaces as mentioned above [15,16], and then resulting in different photoreactivities, which will be further discussed in the following sections.

As for {0 1 0} facets, it has been reported that the reconstruction should introduce a surface with {1 0 1} microfaceted grooves running in the [0 1 0] direction on {0 1 0} facets [32,33]. As a result, some saturated Ti6c atoms would form on the reconstructed {0 1 0} facets because an ideal {1 0 1} facet contain 50% Ti5c and 50% Ti6c atoms, and the percentage of unsaturated Ti5c atoms on the reconstructed {0 1 0} facets would be lower than that on an ideal {0 1 0} ones containing 100% Ti5c atoms [20,35]. It is conventional understanding that those facets with a higher percentage of unsaturated coordinated atoms are usually more reactive in heterogeneous reactions, hence the reconstructed {0 1 0} facets should have lower photoactivity than the unreconstructed {0 1 0} ones, this hypothesis is consistent with the above experimental data shown in Figs. 4 and 5. Namely, Pt-loading under the present intense UV-light irradiation can retard the photocatalytic CO_2 reduction activity of the {0 1 0} facets (TiO_2-0 1 0). Moreover, it has been proved that the b-CO_3^{2-} is easily formed when the CO_2 molecule is bonded to two Ti6c and one O3c surface atoms on the {1 0 1} facets [35], which also can be observed from the ATR-IR spectra shown in Figs. 6a and 7a. As can be seen, the ATR-IR spectrum (Fig. 7a) of the TiO_2-0 1 0-1%Pt shows obviously IR peaks of the adsorbed b-CO_3^{2-}, while the corresponding peaks of b-CO_3^{2-} are very weak as shown in the ATR-IR spectrum (Fig. 6a) of the TiO_2-0 1 0 because there are none of those saturated Ti6c atoms formed in this sample without Pt-loading. This phenomenon can validate the hypothesis on the surface reconstruction of {0 1 0} facets under the present intense UV-light irradiation as mentioned above.

As for TiO_2-0 0 1 facets, it has been theoretically discussed in the 1×4 reconstruction on {0 0 1} in terms of the "ad-molecule" (ADM) model, in which rows of bridging oxygen atoms are replaced with rows of TiO_3 species forming a chain, which gives rise to more additional under-coordinated Ti4c atoms formed on the {0 0 1} facets surface besides its original 100% Ti5c atoms [20]. As mentioned above, a higher percentage of unsaturated coordinated atoms usually mean more reactivity in heterogeneous reaction [20], and therefore the reconstructed {0 0 1} facets should have higher photoactivity than the unreconstructed {0 0 1} ones. This assumption is also confirmed by the experimental results shown in Figs. 4 and 5. Namely, Pt-loading under the present intense UV-light irradiation can significantly promote the photocatalytic CO_2 reduction activity of TiO_2-0 0 1. Moreover, the ATR-IR spectrum (Fig. 7a) of TiO_2-0 0 1-1%Pt was still dominated by m-CO_3^{2-} and HCO_3^- adsorption but without obvious b-CO_3^{2-} adsorption peaks due to the absence of Ti6c, which is different from the situation of the reconstruction of {0 1 0} facets as mentioned above.

Up to now, the above discussion on the effects of the facet reconstruction on the photoactivity is supported by the comparison of the experimental results between the corresponding facets with and without Pt-loading. To eliminate the effects of the Pt-loading, both {0 1 0} and {0 0 1} facets without Pt-loading were also

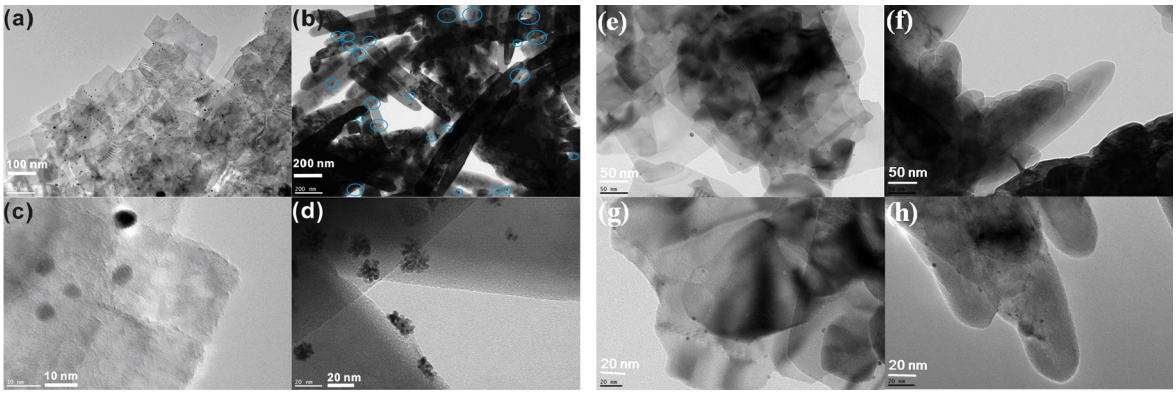

Fig. 8. TEM images of TiO_2-0 0 1-1%Pt (a and c), TiO_2-0 1 0-1%Pt (b and d), TiO_2-0 0 1-0.2%Pt (e and g) and TiO_2-0 1 0-0.2%Pt (f and h).

prepared by using the same intensive UV-light illumination as the Pt-loading process but without addition of H_2PtCl_6 solution. These irradiated facets (without Pt-loading) were also used as photocatalyst to determine their photoactivity at the same condition, and the corresponding results are also listed in Fig. 5. As compared to the corresponding unirradiated one, the irradiated {0 0 1} facets without Pt-loading still show a higher photoactivity (Fig. 5a), while the irradiated {0 1 0} facets have a slightly lower one (Fig. 5b). These changing trends in photoactivity for the irradiated facets are similar to the above observation though the change degrees are much lower as compared to the corresponding Pt-loaded products. Moreover, the ATR-IR spectra (Fig. 7d) of the irradiated TiO_2-0 0 1 and TiO_2-0 1 0 are also very similar to that of their corresponding Pt-loaded ones (Fig. 7a), but obviously different from the unirradiated ones (Fig. 6a), also implying that the reconstruction of those facets lead to the differences in the adsorption of CO_2 regardless of Pt-loading or not. Although there is no direct proof on the reconstruction of the anatase facets under irradiation up till now, the present results give strong evidences on the above assumption that the surface reconstruction could improve the photoactivity of {0 0 1} facets but restrain the photoactivity of {0 1 0} facets.

After comparing and analyzing the IR peak intensities of ATR-IR and the CO_2 desorption peak areas of the CO_2-TPD curves shown in Fig. 7a and b, it can be found that there is no obvious difference between TiO_2-0 1 0-1%Pt and TiO_2-0 0 1-1%Pt on the CO_2 adsorption capability. Therefore, the different effects of Pt-loading on the photoactivity for the two facets should stem from the changes in the photogenerated charge lifetimes as shown in Fig. 7c. By carefully checking the TEM images (Fig. 8) of those Pt-loaded TiO_2 samples, it can be found that the Pt nanoparticles were uniformly and regularly deposited on TiO_2-0 0 1 surfaces (Fig. 8a and c), while the Pt nanoparticles agglomerated on TiO_2-0 1 0 surfaces (Fig. 8b and d). The average diameter of the Pt nanoparticles on TiO_2-0 0 1 can be estimated to be *ca.* 4–5 nm, much smaller than that (~20 nm) of the Pt agglomeration on TiO_2-0 1 0. It has been reported that noble metals such as Au nanoparticles showed a similar size effect on the Fermi level equilibration of semiconductors, where smaller Au nanoparticles can shift the Fermi level of TiO_2 to more negative potentials, leading to an enhanced photocatalytic performance [36,37]. Therefore, the highly uniform Pt nanoparticles on TiO_2-0 0 1 surfaces can effectively transfer the photogenerated electrons and restrain the photogenerated carrier recombination, resulting in the improved photoactivity, while those Pt aggregates on the {0 1 0} facets may not only trap the photogenerated electrons but also consume the holes, and thus serve as recombination centres to restrain the photoactivity [15,16].

By considering that those Pt aggregates on the {0 1 0} facets may stem from the high Pt-loading amount (1 wt%) and H_2PtCl_6 (0.077 M) concentration during the present Pt deposition process, much lower Pt-loading amount (0.2 wt%) and H_2PtCl_6 (0.008 M) concentration were tried to deposit smaller not aggregated Pt particles on {0 1 0} facets (TiO_2-0 1 0-0.2%Pt). For comparison, TiO_2-0 0 1-0.2%Pt was also prepared through the same process. TEM images (Fig. 8e and g) of TiO_2-0 0 1-0.2%Pt are similar to the situation observed from TiO_2-0 0 1-1%Pt (Fig. 8a and c), its surfaces also contain uniformly deposited Pt nanoparticles but with fewer and smaller (*ca.* 2–3 nm) sizes; while TiO_2-0 1 0-0.2%Pt also shows uniformly deposited Pt nanoparticles with small sizes (*ca.* 4–6 nm) on TiO_2-0 1 0 surfaces (Fig. 8e and h), which is significantly different from the TiO_2-0 1 0-1%Pt (Fig. 8b and d). Namely, highly uniform Pt nanoparticles with fewer amount and smaller sizes can be successfully loaded on both the facets. Therefore, the resultant products were also used as photocatalyst to evaluate their photoactivity at the same condition, and the corresponding results are listed in Fig. 5. As can be seen, TiO_2-0 0 1-0.2%Pt shows an obvious enhancement in the photoactivity as compared to the unloaded one, which is similar to TiO_2-0 0 1-1%Pt and TiO_2-0 0 1-5%Pt (Fig. 5a); whereas TiO_2-0 1 0-0.2%Pt has the highest photoactivity among the tested samples such as TiO_2-0 1 0-1%Pt, TiO_2-0 1 0-5%Pt and TiO_2-0 1 0 (Fig. 5b). Obviously, the opposite change in the photoactivity for the 0.2 wt% Pt-loaded TiO_2-0 1 0 as compared to the 1 wt% and 5 wt% Pt-loaded ones can be ascribed to their different morphology and sizes of the loaded Pt particles as shown in Fig. 8. Namely, highly uniform Pt nanoparticles loaded on the {0 1 0} facets can also effectively transfer the photogenerated electrons and restrain the photogenerated carrier recombination, and then improve its photoactivity. Although 0.2 wt% Pt-loading is not reverse of the photoactivity order of {0 0 1} and {0 1 0} facets for the photoreduction of CO_2 to CH_4 since TiO_2-0 1 0-0.2%Pt shows a slightly higher activity than TiO_2-0 0 1-0.2%Pt, the difference in the photoactivity between the two facets is significantly reduced as compared to the unloaded ones (Fig. 5). That is, highly uniform Pt nanoparticles are more benefited to the improvement of the photoactivity of the {0 0 1} facets as compared to the {0 1 0} ones. Moreover, as compared to {0 0 1} facets, {0 1 0} facets with a Pt-loading amount larger than 1 wt% are easier to form Pt aggregates on the surfaces due to their different surface electronic structures and reconstructions during the Pt deposition process, and the Pt aggregates on {0 1 0} facets may serve as recombination centres to depress the photoactivity as mentioned above.

The time-resolved PL spectra of the samples shown in Figs. 6c and 7c can further validate the above suggestion. As can be seen, 1 wt% Pt-loading does not obviously enhance the photogenerated charge lifetime for TiO_2-0 1 0 (only 0.02 ns increment), while there is 29% increment (from 0.65 ns to 0.84 ns) of the charge lifetimes for TiO_2-0 0 1 after Pt-loading. It indicates that an appropriate size of the loaded Pt nanoparticles is beneficial for enhancing the photogenerated carrier separation efficiency, resulting in a much

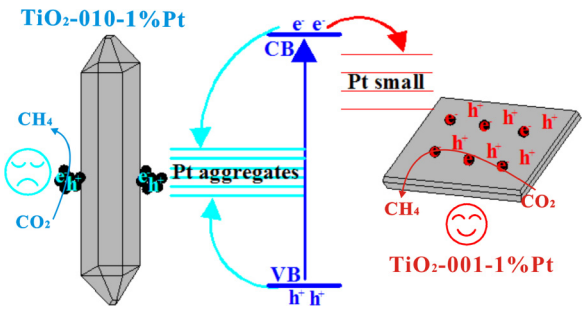

Scheme 1. Possible mechanism of the reversed photoactivity order of anatase TiO_2 {0 0 1} and {0 1 0} facets due to the Pt-loading during the photocatalytic CO_2 reduction process.

longer charge lifetime. According to the CO_2-TPD curves shown in Figs. 6b and 7b, the adsorption peak maximum temperature and the peak areas of the CO_2 desorption from TiO_2-0 0 1 obviously increase after 1 wt% Pt-loading; whereas the corresponding maximum temperature and peak areas of TiO_2-0 1 0 do not increase significantly, indicating that the CO_2 adsorption capability on TiO_2-0 0 1 was enhanced after the Pt-loading, resulting in TiO_2-0 0 1-1%Pt showing a higher photoactivity for the CO_2 reduction. Namely, the above reversed photoactivity order of anatase TiO_2 {0 0 1} and {0 1 0} facets for the photoreduction of CO_2 to CH_4 can be ascribed to changes in the CO_2 adsorption capability and photogenerated carrier separation efficiency on both anatase TiO_2 facets after the Pt-loading.

On the bases of the above-mentioned results on the CO_2 adsorption capability and charge transfer properties on anatase TiO_2 {0 0 1} or {0 1 0} facets, the reversed effect of Pt-loading on the anatase TiO_2 with different facets for the photocatalytic CO_2 reduction was summarized in Scheme 1. The {0 1 0} facets without Pt-loading can strongly adsorb CO_2 molecules with more amount and possesses longer photogenerated charge lifetime than the {0 0 1} facets, resulting in the {0 1 0} facets showing a higher photocatalytic reduction activity of CO_2 to CH_4. After the 1 wt% Pt-loading, the {0 0 1} facets show uniformly and regularly Pt nanoparticles deposited on its surfaces, while the {0 1 0} facets contain Pt nanoparticles agglomerated on the surfaces due to their different surface electronic structures [15,16], and the smaller Pt nanoparticles well-distributed on {0 0 1} facets can more efficiently enhance the photogenerated carrier lifetimes as compared to the agglomerated Pt nanoparticles loaded on {0 1 0} facets, and therefore the TiO_2-0 0 1-1%Pt showed a higher photoactivity for the CO_2 reduction than TiO_2-0 1 0-1%Pt. Moreover, the changes in the CO_2 adsorption capability on anatase TiO_2 {0 0 1} and {0 1 0} facets caused by the reconstruction of the facets during the Pt deposition process also contribute to the above reversed photoactivity order for the CO_2 photoreduction. The present novel phenomenon on the photocatalytic CO_2 reduction activity over anatase TiO_2 with different exposed facets shed light on the fabrication of new photocatalyst with efficient solar energy conversion efficiency for the organic fuel production.

4. Conclusion

In conclusion, the reversed effect of Pt-loading on the photocatalytic CO_2 reduction activity for selectively producing CH_4 over anatase TiO_2 with different facets was demonstrated. The CO_2 adsorption capability and the photogenerated carrier separation efficiency of anatase TiO_2 with {0 1 0} and {0 0 1} facets were discussed to explain the above reversed effect of Pt-loading. Without the Pt-loading, the anatase TiO_2 {0 1 0} facets can strongly adsorb more CO_2 molecules and show longer photogenerated charge lifetime than {0 0 1} facets, and therefore demonstrated a higher photocatalytic reduction efficiency of CO_2 to CH_4. After 1 wt% Pt-loading, the small Pt nanoparticles loaded on TiO_2 {0 1 0} facets can more efficiently enhance the photogenerated carrier separation efficiency as compared to the agglomerated Pt nanoparticles loaded on TiO_2 {0 0 1} facets, and therefore, TiO_2-0 0 1 with 1 wt% Pt-loaded showed a higher photoactivity than TiO_2-0 1 0 loaded with 1wt%Pt. The present results provide an important indication about the effects of Pt-loading on the photocatalytic CO_2 reduction activity of anatase TiO_2 with different exposed facets, and shed light on the fabrication of new photocatalyst with efficient solar energy conversion efficiency for the organic fuel production.

Acknowledgements

This work was supported by National Natural Science Foundations of China (No. 21271146, 21273164, 20973128), and the Large-scale Instrument and Equipment Sharing Foundation of Wuhan University. The authors also acknowledge the assistance from Centre for Electron Microscopy, Wuhan University.

References

[1] C.H. An, J.H. Wang, W. Jiang, M.Y. Zhang, X.J. Ming, S.T. Wang, Q.H. Zhang, Nanoscale 4 (2012) 5646–5650.
[2] C.H. An, J.H. Wang, C. Qin, W. Jiang, S.T. Wang, Y. Li, Q.H. Zhang, J. Mater. Chem. 22 (2012) 13153–13158.
[3] K. Kočí, K. Matějů, L. Obalová, S. Krejčíková, Z. Lacný, D. Plachá, L. Čapek, A. Hospodková, O. Šolcová, Appl. Catal. B Environ. 96 (2010) 239–244.
[4] I.H. Tseng, W.C. Chang, J.C.S. Wu, Appl. Catal. B Environ. 37 (2002) 37–48.
[5] L. Cao, S. Sahu, P. Anilkumar, C.E. Bunker, J. Xu, K.A. Shiral Fernando, P. Wang, E.A. Guliants, K.N. Tackett, Y.P. Sun, J. Am. Chem. Soc. 133 (2011) 4754–4757.
[6] P.W. Pan, Y.W. Chen, Catal. Commun. 8 (2007) 1546–1549.
[7] E.E. Barton, D.M. Rampulla, A.B. Bocarsly, J. Am. Chem. Soc. 130 (2008) 6342–6344.
[8] S.C. Yan, H. Yu, N.Y. Wang, Z.S. Li, Z.G. Zou, Chem. Commun. 48 (2012) 1048–1050.
[9] G.H. Dong, L.Z. Zhang, J. Mater. Chem. 22 (2012) 1160–1166.
[10] Y. Zhou, Z.P. Tian, Z.Y. Zhao, Q. Liu, J.H. Kou, X.Y. Chen, J. Gao, S.C. Yan, Z.G. Zou, ACS Appl. Mater. Interfaces 3 (2011) 3594–3601.
[11] H. Park, J.H. Choi, K.M. Choi, D.K. Lee, J.K. Kang, J. Mater. Chem. 22 (2012) 5304–5307.
[12] W.B. Hou, W.H. Hung, P. Pavaskar, A. Goeppert, M. Aykol, S.B. Cronin, ACS Catal. 1 (2011) 929–936.
[13] Y.P. Xie, G. Liu, L.C. Yin, H.M. Cheng, J. Mater. Chem. 22 (2012) 6746–6751.
[14] J. Pan, X. Wu, L.Z. Wang, G. Liu, G.Q. Lu, H.M. Cheng, Chem. Commun. 47 (2011) 8361–8363.
[15] W.N. Wang, W.J. An, B. Ramalingam, S. Mukherjee, D.M. Niedzwiedzki, S. Gangopadhyay, P. Biswas, J. Am. Chem. Soc. 134 (2012) 11276–11281.
[16] S.C. Chan, M.A. Barteau, Langmuir 21 (2005) 5588–5595.
[17] X. Han, Q. Kuang, M. Jin, Z. Xie, L. Zheng, J. Am. Chem. Soc. 31 (2009) 3152–3155.
[18] L. Sun, Y. Qin, Q.Q. Cao, B.Q. Hu, Z.W. Huang, L. Ye, X.F. Tang, Chem. Commun. 47 (2011) 12628–12630.
[19] F. Amano, T. Yasumoto, O.P. Mahaney, S. Uchida, T. Shibayamad, B. Ohtaniab, Chem. Commun. 45 (2009) 2311–2313.
[20] J. Pan, G. Liu, G.Q. Lu, H.M. Cheng, Angew. Chem. Int. Ed. 50 (2011) 2133–2137.
[21] A. Kubacka, M. Fernandez-García, G. Colón, Chem. Rev. 112 (2012) 1555–1614.
[22] J. Baltrusaitis, J. Schuttlefieldb, E. Zeitler, V.H. Grassiana, Chem. Eng. J. 170 (2011) 471–481.
[23] H. He, P. Zapol, L.A. Curtiss, Energy Environ. Sci. 5 (2012) 6196–6205.
[24] W. Su, J. Zhang, Z. Feng, T. Chen, P. Ying, C. Li, J. Phys. Chem. C 112 (2008) 7710–7716.
[25] L. Liu, H. Zhao, J.M. Andino, Y. Li, ACS Catal. 2 (2012) 1817–1828.
[26] K. Nomura, Y. Ujihira, T. Hayakawa, K. Takehira, Appl. Catal. A Gen. 137 (1996) 25–36.
[27] K.M. Merz, J. Am. Chem. Soc. 112 (1990) 7973–7980.
[28] K.I. Peterson, W.J. Klemperer, Chem. Phys. 80 (1984) 2439–2445.
[29] M. Primet, P. Pichat, M.V. Mathieu, J. Phys. Chem. 75 (1971) 1220–1221.
[30] A. Yan, B. Liu, Y. Dong, Z. Tian, D. Wang, M. Cheng, Appl. Catal. B Environ. 80 (2008) 24–31.
[31] M. Lazzeri, A. Selloni, Phys. Rev. Lett. 87 (2001) 266105.
[32] N. Ruzycki, G.S. Herman, L.A. Boatner, U. Diebold, Surf. Sci. 529 (2003) L239.
[33] U. Diebold, N. Ruzycki, G.S. Herman, A. Selloni, Catal. Today 85 (2003) 93–100.
[34] G. Liu, J.C. Yu, G.Q. Lu, H.M. Cheng, Chem. Commun. 47 (2011) 6763–6783.
[35] D.C. Sorescu, W.A. Al-Saidi, K.D. Jordan, J. Chem. Phys. 135 (2011) 124701 (17pp).
[36] N. Wang, T. Tachikawa, T. Majima, Chem. Sci. 2 (2011) 891–900.
[37] M. Murdoch, G.I.N. Waterhouse, M.A. Nadeem, J.B. Metson, M.A. Keane, R.F. Howe, J. Llorca, H. Idriss, Nat. Chem. 3 (2011) 4189–4192.